Tuning the Morphology and Performance of Low Bandgap Polymer:Fullerene Heterojunctions via Solvent Annealing in Selective Solvents

*Huipeng Chen, Yu-Che Hsiao, Bin Hu, and Mark Dadmun**

Low bandgap polymer (LBG):fullerene mixtures are some of the most promising organic photovoltaic active layers. Unfortunately, there are no post-deposition treatments available to rationally improve the morphology and performance of as-cast LBG:fullerene OPV active layers, where thermal annealing usually fails. Therefore, there is a glaring need to develop post-deposition methods to guide the morphology of LBG:fullerene bulk heterojunctions towards targeted structures and performance. In this paper, the structural evolution of PCPDTBT:PCBM mixtures with solvent annealing (SA) is examined, focusing on the effect of solvent quality of the fullerene and polymer in the annealing vapor on morphological evolution and device performance. The results indicate that exposure of this active layer to the solvent vapor controls the ordering of PCPDTBT and PCBM phase separation very effectively, presumably by inducing component mobility as the solvent plasticizes the mixture. These results also unexpectedly indicate that solvent annealing in a selective solvent provides a method to invert the morphology of the LBG:fullerene mixture from a polymer aggregate dispersed in a polymer:fullerene matrix to fullerene aggregates dispersed in a polymer:fullerene matrix. The judicious choice of solvent vapor, therefore, provides a unique method to exquisitely control and optimize the morphology of LBG conjugated polymer/fullerene mixtures.

1. Introduction

Conjugated polymer:fullerene blends are benchmark materials for organic photovoltaic (OPV) active layers due to their flexibility, ease of processing, and straightforward thin film formation. A typical bulk heterojunction (BHJ) active layer is formed by casting a thin film from a solution mixture of the donor polymer and acceptor fullerene, where nanoscale interpenetrating networks are ideally formed upon solvent evaporation.[1–8] One of the most studied OPV BHJ blends is the mixture poly(3-hexyl thiophene) (P3HT) and [6,6]-phenyl-C_{61}-butyric acid methyl ester (PCBM), where the as-cast devices often exhibit poor photovoltaic efficiencies. Subsequent processing, such as thermal annealing or solvent vapor annealing are therefore required to allow the morphology of the mixture to evolve towards a structure with improved photovoltaic efficiency.[9–17] Moreover, low bandgap (LBG) polymer/fullerene systems are the most promising conjugated polymer fullerene systems for OPVs. Unfortunately, thermal annealing after deposition does not improve or often decreases the device performance.[18–21] Therefore, the use of additives during film deposition has become a popular method to modify the morphology of LBG/fullerene system in order to enhance the device performance. These additives usually have a higher boiling temperature than the host solvent and selective solubility to PCBM. One of the most studied LBG system is the poly[2,6-(4,4-bis-(2-ethylhexyl)-4*H*-cyclopenta [2,1-*b*;3,4-*b*′]dithiophene)-*alt*-4,7(2,1,3-benzothiadiazole)] (PCPDTBT):PCBM system, often deposited with a solvent additive. The power conversion efficiency (PCE) of PCPDTBT:PCBM BHJ system has been shown to increase from 1.7% to 3.45–4.62% with the addition of a solvent additive.[18] To more fully understand the role of the additive, Russell and coworkers studied the morphology changes of the thin film of a PCPDTBT:PCBM mixture that is deposited from solution with additives, where they found that PCBM aggregation and an increase of PCPDTBT ordering occurred with the presence of solvent additives. They further ascribe these structural changes to an improvement in charge transport, which translates to improved device performance.[18]

While the addition of solvent additives has shown some performance improvement of LBG based organic photovoltaic, the morphology of the as-cast LBG:fullerene film, with or without solvent additives, is locked in from the non-equilibrium deposition process. Therefore, there is still a pressing need to

Dr. H. P. Chen, Prof. M. Dadmun
Department of Chemistry
University of Tennessee
Knoxville, TN 37996, USA
E-mail: Dad@utk.edu
Dr. H. P. Chen
Institute of Optoelectronic Display
Fuzhou University
Fuzhou 350002, PR China
Prof. M. Dadmun
Chemical Science Division
Oak Ridge National Lab
Oak Ridge, TN 37831, USA
Y.-C. Hsiao, Prof. B. Hu
Department of Materials Science and Engineering
University of Tennessee
Knoxville, TN 37996, USA

DOI: 10.1002/adfm.201400552

develop post-deposition methods to *guide* the morphology of LBG:fullerene bulk heterojunctions towards targeted structures and performance. Aside from thermal annealing, solvent annealing (SA) is another post-deposition process to guide the BHJ morphology to evolve to a new structure that improves device performance. SA is a versatile method where a thin film is exposed to an atmosphere of solvent vapors that diffuse into the deposited layer, the extent of which is dependent on and thus controllable by exposure time. With SA, the solvent increases molecular mobility of the components in the active layer, allowing the system to evolve towards a more thermodynamically stable morphology. The improvement of device performance with SA for P3HT/PCBM system has been widely reported.[12–17] Moreover, unlike thermal annealing, where structure develops in seconds and crystallization and phase separation cannot be examined separately, solvent annealing provides more precise morphological control.[22,23] While there has been significant success in controlling the morphology and performance of the P3HT/PCBM system with SA, there has been little work that has focused on understanding how solvent annealing can controllably modify the morphology and performance of the LBG/PCBM system, especially when TA is not an option to improve device performance. Solvent annealing is a promising approach to control the morphology of LBG polymer:fullerene mixtures to fabricate improved and stable solar cell devices, because the morphology evolves by increasing molecular mobility of the components with the inclusion of solvent vapor at room temperature without damaging the polymers and crystallizing PCBM.[22,23] An important parameter in the solvent annealing process that is often overlooked is the selectivity of the solvent vapor to the polymer and fullerene. Many previous studies have focused on mutual solvents for the polymer and fullerene, however the impact of annealing a conjugated polymer:fullerene mixture in the vapor of a solvent that is selective to the fullerene (or polymer) has not been studied. Moreover, one can readily envision that the morphology (and photovoltaic performance) of a conjugated polymer:fullerene thin film that is annealed in a solvent vapor that is selective to the fullerene will differ dramatically from one that is annealed in a solvent vapor that is selective to the polymer. Furthermore, solvent annealing has been widely used to control the morphology of diblock copolymers and solvent quality, as defined by the solubility of each component in the solvent, is known to be an important parameter.[24–28] As both the diblock copolymer and LBG/fullerene systems are multi-component polymer systems, there is little doubt that solvent annealing LBG/fullerene systems in selective solvents will provide a more precise control of the morphology and develop rational post-deposition treatments that will further enable device performance improvement. Clearly, a more thorough understanding of the relationship between solvent selectivity and morphology evolution with solvent vapor exposure is needed. Thus, a fundamental understanding of the development of morphology of LBG polymer:fullerene blends with solvent annealing as a function of solvent selectivity is required for the optimization of the morphology and performance of LBG/PCBM OPV active layers.

The purpose of this study is to investigate the impact of solvent vapor quality on the morphology and device performance of solvent annealed LBG/PCBM systems. In the present work, the changes in morphology of PCPDTBT/PCBM films with SA in a variety of solvent vapors are monitored using small angle neutron scattering (SANS), which is a very effective technique to characterize the morphology of LBG/fullerene thin films due to the significant scattering length density contrast between PCPDTBT and PCBM. To monitor the impact of solvent selectivity on the morphology development, solvent annealing in three different solvents will be examined: one that is selective to PCBM (2-Chlorophenol), a second one that is selective to the PCPDTBT (Bromobenzene), and a third one which has similar solubility to PCBM and the PCPDTBT polymer (ODCB). These results will therefore correlate solvent selectivity to the morphology and performance of the LBG:PCBM system. The structural changes are correlated to the photovoltaic activity of the active layer to provide guidelines by which the active layer of conjugated polymer/fullerene heterojunctions can be optimized with controlled solvent exposure.

2. Results

The solubility of PCPDTBT and PCBM samples in the three solvents of interest are shown in **Table 1**. These results show that 2-chlorophenol (CP) is a selective solvent for PCBM, where the solubility of PCBM in CP is 128 mg/mL while the solubility of PCPDTBT in CP is only 0.2 mg/mL. Similarly, bromobenzene (BB) is demonstrated to be a selective solvent for PCPDTBT, as the solubility of PCBM in BB is 33 mg/mL while the solubility PCPDTBT in BB is 89 mg/mL. Finally, 1,2-dichlorobenzene (ODCB) is shown to be a similar solvent for PCPDTBT and PCBM. The solubility of PCBM in ODCB (36 mg/mL) is slightly higher than that of PCPDTBT in ODCB (21 mg/mL).

The small angle neutron scattering (SANS) curves for the as-cast and solvent annealed PCPDTBT:PCBM samples are presented in **Figure 1**. The scattering of the as-cast (AC) sample is very weak, which is consistent with previous reports, indicating a fairly homogeneous distribution of the fullerene and polymer in this film.[18] The scattering pattern of the sample that is annealed in chlorophenol or ODCB exhibit similar scattering patterns that have stronger scattering at low Q than that of the sample that is annealed in bromobenzene. This increased scattering indicates the formation of structures at this length scale ($2\pi/Q$), which usually indicates phase separation in conjugated polymer/fullerene mixtures.

Figure 2 shows the data as Lorentz-corrected scattering (IQ^2 vs. Q), which accentuates the correlation peaks at Q ~ 0.015 $Å^{-1}$ for the ODCB and CP samples and Q ~ 0.02 $Å^{-1}$ for the BB sample. These peaks correspond to the average distance ($2\pi/Q_{max}$) between two adjacent domains. There is no peak observed for the AC sample, which is consistent with the homogeneous dispersion of PCBM in PCPDTBT. The corresponding distance

Table 1. Solubility of PCPDTBT and PCBM in solvents of interest.

Solvent	Solubility (mg/mL)	
	PCPDTBT	PCBM
Bromobenzene (BB)	89	33
1,2-Dichlorobenzene (ODCB)	21	36
2-Chlorophenol (CP)	0.2	128

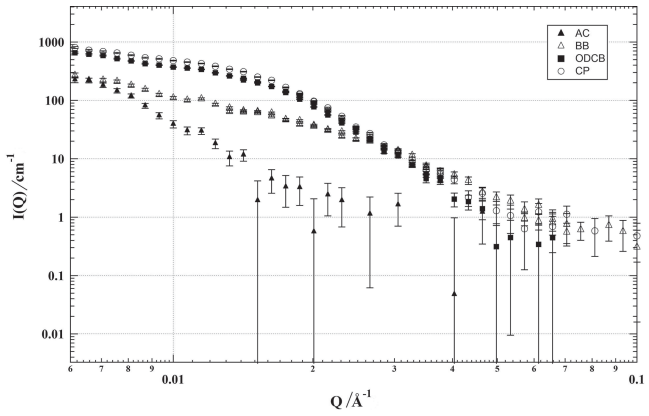

Figure 1. The absolute small angle neutron scattering intensity of the as-cast and solvent annealed samples.

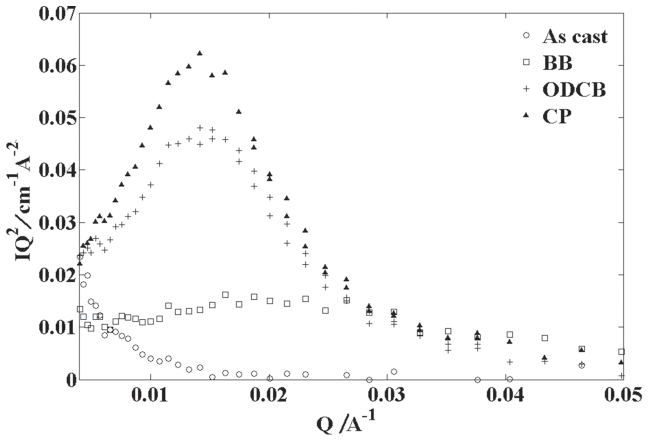

Figure 2. Lorentz-corrected scattering pattern of as-cast and solvent annealed samples.

($2\pi/Q_{max}$) of these samples shows an average distance of ~420 Å between two adjacent domains for the CP and ODCB samples while there is an average distance of ~310 Å between two adjacent domains for the BB sample (**Table 2**). In addition, the correlation peaks of the CP and ODCB samples are much sharper than the BB sample, which means a more narrow distribution of domains exists in the CP and ODCB samples.

There are two possibilities for the phase separation in these samples, the aggregation of PCPDTBT in a surrounding matrix that consists of a mixture of PCPDTBT and PCBM or PCBM domains that are dispersed in a surrounding matrix that consist of a mixture of PCPDTBT and PCBM. A careful quantitative analysis of the scattering curves allows us to differentiate between these two structures.

In neutron scattering, the scattering intensity is proportional to the square of the difference of the scattering length density of the scattering object and its surroundings ($b_1 - b_2$) and the form factor (P(Q)) of the scattering object, $I(Q) \sim (b_1 - b_2)^2 P(Q)$. The scattering curves were first fit with the assumption that the form factor is modeled by the Schulz sphere model.[22,29,30] This form factor describes a two-phase system that contains a pure phase of spherical domains that have a Schulz size distribution and are dispersed in the matrix of the other phase. In the solvent annealed samples, these two phases correspond to the dispersed aggregated phase surrounded by a mixture of PCPDTBT and PCBM.

This fitting allows the comparison of the scattering length density difference ($b_1 - b_2$) between the dispersed spheres and the surrounding matrix to that which is consistent with the composition of the cast film. This analysis begins by fitting the scattering curves of the ODCB and CP annealed samples to the Schulz sphere model, Shown in **Figure 3**. Assuming that the spherical domains consist of PCPDTBT, which has an SLD (b_1) of 1.1×10^{-6} Å^{-2}, the dispersed domain radius, volume fraction of the dispersed domain in the whole sample ($w^{fit}_{agg,P}$), and SLD of the surrounding matrix (b_2) are readily obtained and are listed in Table 2.

Knowledge of the scattering length density of the surrounding matrix and the composition of the film provides an orthogonal method to calculate the volume fraction of the dispersed phase in the whole sample ($w^{cal}_{agg,P}$) by the procedure described below. This provides a self-consistent check to the assumption that the dispersed domains consist of PCPDTBT; $w^{fit}_{agg,P} = w^{cal}_{agg,P}$ if the dispersed domains are PCPDTBT and $w^{fit}_{agg,P} \neq w^{cal}_{agg,P}$ if they are not.

To determine $w^{cal}_{agg,P}$, the volume fraction of PCPDTBT in the surrounding mixed phase ($\Phi_{P,m}$) is calculated by Equation (1):

$$\phi_{P,m} = \frac{SLD_{PCBM} - SLD_m}{SLD_{PCBM} - SLD_{PCPDTBT}} \quad (1)$$

where SLD_{PCBM} and $SLD_{PCPDTBT}$ are scattering length densities of PCBM and PCPDTBT, respectively, and SLD_m is the SLD of the surrounding matrix (b_2). In this case, all of the PCBM is in surrounding matrix, so the volume fraction of PCPDTBT in the surrounding phase in the whole sample (w_P,m) is found by Equation (2).

$$w_{P,m} = w_{PCBM} \times \frac{\phi_{P,m}}{1-\phi_{P,m}} \quad (2)$$

Finally, the volume fraction of the dispersed phase in the whole sample ($w^{cal}_{agg,P}$) is calculated by Equation (3):

$$w^{cal}_{agg,P} = w_p - w_{P,m} = 0.4 - w_{PCBM} \times \frac{\phi_{P,m}}{1-\phi_{P,m}} \quad (3)$$

Table 2. Structure parameters obtained from Schulz sphere model and calculation with the assumption that the aggregates are PCPDTBT.

PCPDTBT Aggregates	$w^{fit}_{agg,P}$	SLD contrast ($\times 10^{-6}$ Å^{-2})	Aggregate SLD ($\times 10^{-6}$ Å^{-2})	Matrix SLD ($\times 10^{-6}$ Å^{-2})	$\Phi_{P,m}$	$w_{P,m}$	$w^{cal}_{agg,P}$
CP	0.225	1.70	1.1	2.8	0.48	0.55	–0.15
ODCB	0.205	1.65	1.1	2.75	0.50	0.60	–0.20

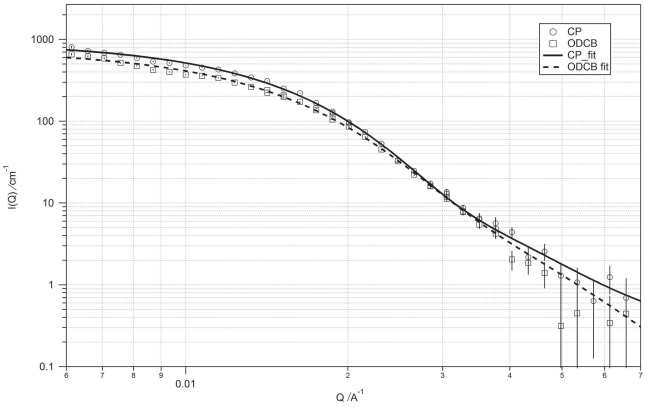

Figure 3. Fit of the form factor of the samples that are solvent annealed in ODCB and CP vapor to the scattering of a Schulz sphere. Parameters extracted from these fits are given in Table 2 and Table 3.

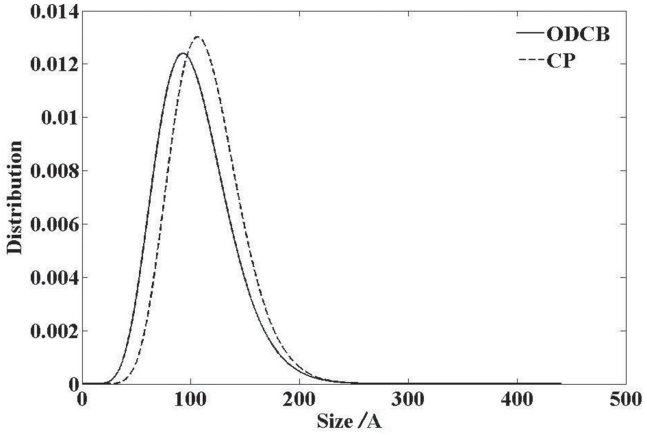

Figure 4. Size distribution of PCBM aggregates in the samples that are solvent annealed in ODCB and CP vapor.

where w_{PCBM} and w_P are the volume fraction of PCBM and PCPDTBT in the whole sample, which are 0.6 and 0.4 respectively. The results of this analysis when assuming the aggregates are PCPDTBT are shown in Table 2, where brief inspection clearly shows that $w_{agg,P}^{fit} \neq w_{agg,P}^{cal}$, and thus, the aggregates cannot be PCPDTBT.

Therefore, the identical analysis was completed on the Schulz sphere model fits but assuming that the aggregates are PCBM, which has an SLD (b_1) of 4.4×10^{-6} Å^{-2}. From these fits, the dispersed domain radius, dispersed domain vol% in the whole sample ($w_{agg,PCBM}^{fit}$) and SLD of the surrounding matrix (b_2) are obtained and listed in **Table 3**.

As described above, the volume fraction of the dispersed phase in the whole sample (w_{agg}^{cal}) can then be calculated based on the scattering length density of the surrounding matrix that comes from the fitted scattering curve. In a similar manner to the analysis described above, the volume fraction of PCBM in the surrounding mixed phase ($\Phi_{PCBM,m}$) is calculated by Equation (4)

$$\phi_{PCBM,m} = \frac{SLD_m - SLD_{PCPDTBT}}{SLD_{PCBM} - SLD_{PCPDTBT}} \quad (4)$$

In this case, all of the PCPDTBT is in surrounding matrix, so the volume fraction of PCBM in the surrounding phase in the whole sample (w_{PCBM},m) is obtained by Equation (5)

$$w_{PCBM,m} = w_{PCPDTBT} \times \frac{\phi_{PCBM,m}}{1-\phi_{PCBM,m}} \quad (5)$$

Thus, the volume fraction of the dispersed phase is determined by Equation (6):

$$w_{agg,PCBM}^{cal} = w_{PCBM} - w_{PCBM,m} = 0.6 - w_{PCPDTBT} \times \frac{\phi_{PCBM,m}}{1-\phi_{PCBM,m}} \quad (6)$$

The results of this analysis when assuming that the dispersed phase is PCBM are shown in Table 3, where the agreement of $w_{agg,PCBM}^{fit}$ and $w_{agg,PCBM}^{cal}$ indicates the aggregates are PCBM.

Thus, this careful quantitative analysis of the SANS data shows that the samples that are annealed in a solvent that is preferable to PCBM (CP) forms a film with phase separated PCBM domains that make-up 22 vol% of the sample, with an average domain size of 115 Å. Similarly, the sample that is annealed in the vapor of a solvent that is close to a mutual solvent for PCBM and PCPDTBT also forms a film with PCBM precipitates that constitute 20 volume percent of the sample and are 104 Å in size. The distributions of the PCBM domain size that is based on the Schulz distributions are presented in **Figure 4**, which shows most PCBM aggregates are 100 ± 50 Å in size.

The scattering curve of the sample that is annealed in bromobenzene vapor exhibits a scattering pattern that differs from all other samples and does not fit the Schulz sphere model. This scattering curve is thus fit to an elliptical cylinder model, which describes a two-phase system that consists of a pure phase with an elliptical cylinder shape that is dispersed in a surrounding matrix, and has been successful in fitting conjugated polymer:fullerene mixtures.[22,31,32] This fit is shown in **Figure 5**, from which the size of the dispersed elliptical cylinders, the volume fraction of the dispersed phase in the whole sample and the scattering length density of the surrounding matrix (b_2) are determined.

Moreover, a similar self-consistent check of the identity of the dispersed phase, PCPDTBT or PCBM, can be completed by calculating the volume fraction of dispersed phase (w_{agg}^{cal}) and comparing it to the volume fraction of the dispersed phase that comes from the fitting procedure (w_{agg}^{fit}). Equations (1–3) are implemented to determine $w_{agg,P}^{cal}$ assuming that the aggregates

Table 3. Structure parameters obtained from Schulz sphere model and calculation with the assumption that the aggregates are PCBM.

PCBM Aggregates	$w_{agg,PCBM}^{fit}$	SLD contrast ($\times 10^{-6}$ Å^{-2})	Aggregate SLD ($\times 10^{-6}$ Å^{-2})	Matrix SLD ($\times 10^{-6}$ Å^{-2})	$\Phi_{PCBM,m}$	$w_{PCBM,m}$	$w_{agg,PCBM}^{cal}$
CP	0.225	1.70	4.4	2.70	0.48	0.37	0.23
ODCB	0.205	1.65	4.4	2.75	0.50	0.40	0.20

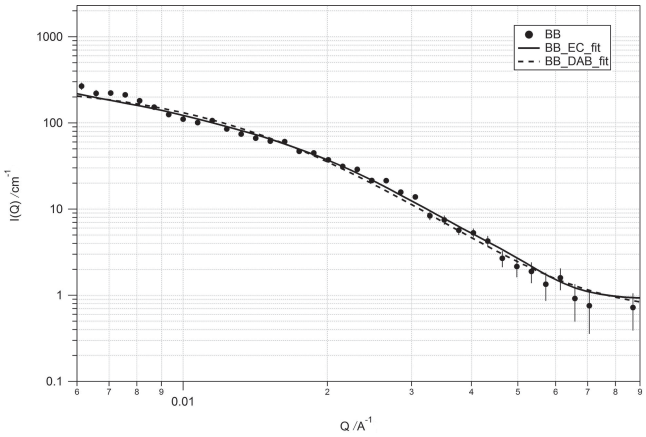

Figure 5. Fit of the sample that is solvent annealed in BB vapor to the scattering of an elliptical cylinder (BB_EC_fit) and the Debye-Bueche model (BB_DAB_fit). Parameters extracted from these fits are given in Table 4.

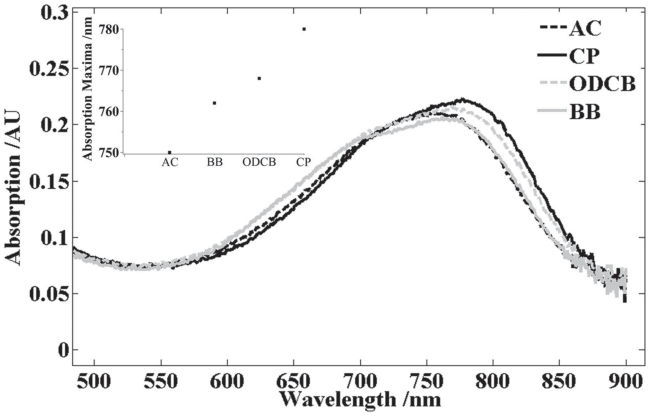

Figure 6. UV-vis spectra for the as-cast and solvent annealed samples. The inset shows the absorption maxima for all the samples.

are PCPDTBT, while Equation (4–6) provide $w^{cal}_{agg,PCBM}$ assuming that the aggregated phase is PCBM. The results of these analyses are shown in **Table 4**, where the agreement of $w^{cal}_{agg,P}$ and $w^{fit}_{agg,P}$ indicates the aggregates are PCPDTBT. These results also show that the aggregates are 157 Å and constitute 7 vol% of the sample.

The structure of the sample that is annealed in bromobenzene vapor is further verified by fitting the scattering curve to the Debye-Bueche Equation, which generically models a two-phase system with sharp interfaces and is shown in Equation (7).[33,34]

$$I(Q) = I_0 \left(1/Q^2\xi^2\right)^2 \quad (7)$$

In Equation (7), ξ is the correlation length of the system and I_0 is the zero-angle scattering intensity, which is dependent on the scattering length densities of the two phases and their volume fractions.

$$I_0 = 8\pi(b_1 - b_2)^2 w_{agg}(1-w_{agg})\xi^3 \quad (8)$$

In Equation (8), w_{agg} is the volume fraction of the dispersed phase in the whole sample; b_1-b_2 is the scattering length density contrast between the dispersed phase and the surrounding mixed phase. If the dispersed phase is PCPDTBT, then

$$b_1 - b_2 = SLD_{PCPDTBT} - \frac{SLD_{PCBM} * w_{PCBM} + SLD_{PCPDTBT} * (w_{PCPDTBT} - w_{agg})}{1 - w_{agg}} \quad (9)$$

which is only dependent on the volume fraction of the dispersed PCPDTBT, w_{agg}. Thus, w_{agg} can be calculated from I_0 that comes from the fitting procedure using Equations (8) and (9). This analysis indicates that the sample that is annealed in bromobenzene vapor consists of PCPDTBT aggregates which constitute 7 vol% of the sample, which is in excellent agreement with the analysis of the fitting of the scattering curve to the form factor of an elliptical cylinder.

While SANS provides information on the morphology of the PCPDTBT/PCBM mixtures, UV-Vis spectroscopy provides information on the orientational order of the polymer in the samples, and this can monitor how solvent annealing alters the local order of the PCPDTBT in these samples. The UV-vis spectra of the as-cast and solvent annealed samples are shown in **Figure 6**. The as-cast sample exhibits a maximum in absorption at 750 nm, however there is a red shift in this maximum to 780 nm after solvent annealing in chlorophenol, a sample with PCBM aggregates. This red shift has been ascribed to either an interchain-delocalization or a planarization of the polymer backbone, resulting in an increased π–π conjugation length and a higher degree of ordering.[18,35–37] The sample that is solvent annealed in ODCB exhibits a red shift as well, to 768 nm, indicating an increase in order of the polymer, but not as much as for the sample that is solvent annealed in chlorophenol. The sample that is annealed in bromobenzene vapor, which SANS indicates consists of aggregated PCPDTBT domains, exhibits a blue shift of the absorption, which indicates a decrease in the degree of ordering of the polymer after solvent annealing in BB.

The results reported above clearly document the change of structure with solvent annealing. The sample that is annealed

Table 4. Structure parameters obtained from elliptical cylinder model and calculation with the assumption that the aggregates are either PCBM or PCPDTBT.

Aggregate	$w^{fit}_{agg,PCBM}$	SLD contrast ($\times10^{-6}$ Å^{-2})	Aggregates SLD ($\times10^{-6}$ Å^{-2})	Matrix SLD ($\times10^{-6}$ Å^{-2})	$\Phi_{PCBM,\,m}$	$w_{PCBM,\,m}$	$w^{cal}_{agg,PCBM}$
PCBM	0.07	2.13	4.4	2.27	0.35	0.22	0.38
Aggregate	$w^{fit}_{agg,P}$	SLD contrast ($\times10^{-6}$ Å^{-2})	Aggregates SLD ($\times10^{-6}$ Å^{-2})	Matrix SLD ($\times10^{-6}$ Å^{-2})	$\Phi_{P,\,m}$	$w_{P,\,m}$	$w^{cal}_{agg,P}$
PCPDTBT	0.07	2.13	1.1	3.23	0.35	0.33	0.07

in CP vapor exhibits an increase in PCPDTBT ordering and precipitation of a separate PCBM phase, while the sample that is annealed in ODCB vapor also exhibits an increase in PCPDTBT ordering and PCBM aggregates, but the extent of PCPDTBT ordering is less than that of the CP annealed sample. Finally, the sample that is annealed in bromobenzene vapor exhibits a decrease in PCPDTBT ordering, contains PCPDTBT aggregates, but no PCBM precipitates. In order for this information to be most useful, these structural changes must be correlated to OPV function. With this in mind, the photovoltaic properties of all the samples were determined. These results are shown in **Table 5** and **Figure 7**. These results indicate that there is no improvement from the as-cast sample in power conversion efficiency (PCE) after solvent annealing in bromobenzene. Annealing in ODCB or CP, however, do show an increase in short-circuit current (J_{SC}), fill factor (FF), and PCE, where the PCE increased to 3.5% after solvent annealing in CP. This represents an increase in PCE of 75% and is comparable to the PCE obtained when processing PCPDTBT/PCBM samples with solvent additive; Russell and coworkers reported an increase PCE from 1.68% to 3.45%–4.62% with the addition of solvent additives.[18]

3. Discussion

The controlled exposure of PCPDTBT:PCBM mixture to solvent vapor clearly alters the morphology of the mixture layer, where the morphology of the thin film can be inverted by the judicious choice of solvent quality of the annealing vapor. Surprisingly, exposure of the conjugated polymer:fullerene mixture to a solvent that is selective for the fullerene (CP) results in the precipitation of the fullerene in the final film. Similarly, the exposure of the thin film to a solvent that is preferable for the polymer (BB) forms a morphology with polymer aggregates. This is surprising because one would expect that the preferred solute would precipitate *after* the non-preferred solute if the solvent-solute interactions dominate the morphology development. Thus, these results indicate that the interactions between PCPDTBT and PCBM, rather than the interactions between either of these components and the solvent, dominate the morphology development in the solvent annealing process. It is also clear that the choice of annealing solvent vapor mitigates these interactions and thus directs the morphology development as well.

These results also demonstrate that the exquisite control of the PCPDTBT morphology with solvent annealing also dramatically impacts its ability to act as an active layer in an organic photovoltaic device. With solvent vapor annealing, the PCPDTBT

Table 5. Device performance at standard AM-1.5 illumination.

	V_{OC} [V]	J_{SC} [mA/cm^2]	FF [%]	PCE [%]
AC	0.60 ± 0.01	6.87 ± 0.2	48 ± 1	2.0 ± 0.1
BB	0.58 ± 0.01	7.47 ± 0.2	47 ± 1.5	2.0 ± 0.1
ODCB	0.58 ± 0.01	8.48 ± 0.3	52 ± 1	2.6 ± 0.1
CP	0.59 ± 0.01	9.90 ± 0.2	59 ± 1	3.5 ± 0.1

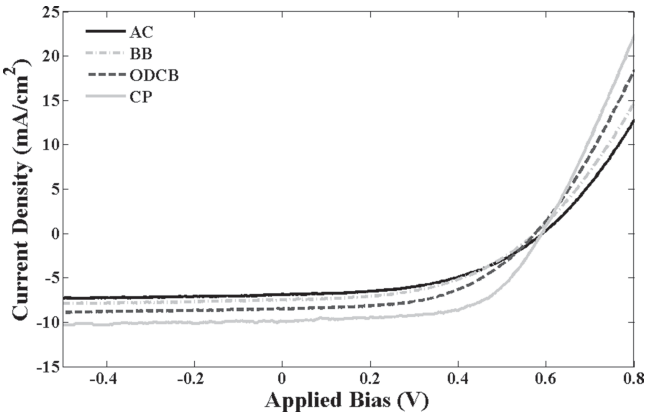

Figure 7. Current density vs. applied voltage curves for the as-cast and solvent annealed samples.

and PCBM molecules become more mobile, resulting in a reorganization of active layer. Most importantly, the resultant morphology of the active layer with SA can be precisely guided by the choice of solvent quality of the annealing vapor.

The structure of the thin film is dominated by the deposition process in the as-cast sample, resulting in the relatively homogeneous distribution of PCBM throughout the sample, as verified by the SANS results. With solvent annealing in bromobenzene, in which PCPDTBT is selectively soluble, the solvent incursion into the film drives the PCPDTBT chains to aggregate, resulting in a film with 7 vol% PCPDTBT aggregates dispersed in a homogeneous mixture of PCPDTBT and PCBM. Moreover, the selective solubility of PCPDTBT in BB appears to interrupt some PCPDTBT ordering in the as-cast film, resulting in less ordered PCPDTBT chains with SA, which is verified by UV-vis.

With solvent annealing in ODCB vapor, in which PCBM and PCPDTBT are similarly soluble, the PCPDTBT matrix is swollen with the solvent. The increased molecular mobility with exposure to vapor guides the PCPDTBT chains to form a more ordered structure, as indicated by UV-vis. Moreover, the higher degree of PCPDTBT ordering appears to facilitate the phase separation of PCBM from PCPDTBT. The similar solubility of PCPDTBT and PCBM offers sufficient mobility to the PCBM molecule for it to evolve towards thermodynamically favorable larger aggregates and phase separation. This is consistent with our previous work in which enhanced P3HT crystallization and PCBM phase separation occurs after 90 minutes of solvent annealing in ODCB, in which P3HT and PCBM also have similar solubility.[22]

With solvent annealing in chlorophenol vapor, in which PCBM is selectively soluble, the incursion of solvent appears to extract PCBM from the homogeneous as-cast PCPDTBT/PCBM mixture due to the high solubility of PCBM in CP. This then evolves to form a film with 23 vol% PCBM aggregates, as verified by the SANS results. This phase segregation is accompanied by an increase in the ordering of the PCPDTBT molecules, as demonstrated by UV-vis.

The control of morphology of the active layer dramatically impacts its photovoltaic performance, and these morphological

alterations are correlated to OPV performance. SA in BB vapor, in which PCPDTBT is selectively soluble, forms a film with 7 vol% PCPDTBT aggregates, a lower degree of PCPDTBT ordering, and no PCBM aggregates. This morphology does not improve device performance relative to the as-cast film. The morphologies that are formed by solvent annealing in ODCB or CP, however, do improve device performance. SA in ODCB vapor, in which PCPDTBT and PCBM have similar solubility, forms a morphology with increased PCPDTBT ordering and 20 vol% PCBM aggregates. The enhanced PCPDTBT ordering facilitates hole transport and the presence of the pure PCBM phase facilitates electron transport, which increases PCE by 30%. The highest degree of PCPDTBT ordering is obtained after SA the film in CP, in which PCBM is selectively soluble. This film also contains 23 vol% PCBM aggregates. This morphology increases the PCE by 75% relative to the as-cast film. These results therefore, clearly indicate that sufficient PCPDTBT ordering and the formation of a PCBM pure phase are crucial in the optimization of the morphology of the PCPDTBT:PCBM active layer.

A crucial implication of these results is that the solvent quality in the solvent annealing process provides a controllable and versatile method to direct the morphology of a conjugated polymer:fullerene nanocomposite, enabling the optimization of the morphology of LBG:fullerene active layers. This is particularly important as thermal annealing usually fails to improve the performance of LBG:fullerene systems. The exquisite morphological control that is afforded by this process also offers a more detailed understanding of the structural development in LBG polymer based OPV bulk heterojunctions and provides a unique method to control and optimize the morphology of the LBG conjugated polymer/fullerene mixture. Moreover, this procedure will be broadly applicable to controlling the morphology of a broad range of promising polymer nanocomposites as next-generation functional materials.

4. Conclusion

The structural development of a PCPDTBT:PCBM mixture with controlled exposure to solvent vapor with varying PCPDTBT and PCBM solubility is examined. The results indicate that exposure of this active layer to the solvent vapor alters the ordering of PCPDTBT and PCBM phase separation very effectively, presumably by inducing mobility of the components as the solvent plasticizes the mixture. These results unexpectedly show that the morphology of the polymer:fullerene mixture can be inverted from a film that consists of polymer aggregates dispersed in a polymer:fullerene matrix to a film that consists of fullerene domains that are dispersed in a polymer:fullerene matrix by the selective solubility of the polymer and fullerene in the annealing vapor. These results therefore require that the interactions between PCPDTBT and PCBM, rather than the interactions between either of these components and the solvent, dominate the morphology development in the solvent annealing process.

This exquisite control of morphology clearly demonstrates that sufficient PCPDTBT ordering and the formation of a pure PCBM phase are crucial in optimizing the performance of PCPDTBT:PCBM OPV active layers. Moreover, as thermal annealing is typically unsuccessful in improving the morphology of low bandgap polymer:fullerene OPV active layers, solvent annealing provides a unique method to carefully control and optimize the morphology of the LBG conjugated polymer/fullerene mixture. Furthermore, this process is broadly applicable to a broad range of promising polymer nanocomposites to control morphology and function.

More importantly, the judicious choice of solvent vapor for solvent annealing provides a level of morphological control in conjugated polymer:fullerene mixtures that has not been previously available. This novel process, therefore, precisely guides the morphology development in OPV active layers and offers a promising process to more accurately correlate the active layer morphology and photovoltaic performance.

5. Experimental Section

Materials: [6,6]-Phenyl-C_{61}-butyric acid methyl ester (PCBM) was purchased from Nano-C, and (PCPDTBT) (M_W = 41K, PDI = 2.3) was purchased from 1-Materials. Both are used without further purification. To fabricate the PCPDTBT/PCBM films, PCPDTBT (7 mg/mL) and PCBM (14 mg/mL) were dissolved in *o*-dichlorobenzene (ODCB). Prior to spin-coating, the silicon wafers are cleaned by immersion in a 3:1 (v/v) mixture of concentrated sulfuric acid and 30% (v/v) hydrogen peroxide, heated to ~70 °C for 15 min, and rinsed with copious amounts of high purity water and dried under a stream of nitrogen. The photovoltaic active layer PCPDTBT:PCBM mixture was fabricated by spin casting a thin film from the PCPDTBT/PCBM solution at 800 rpm for 5 s, followed by 300 rpm for 300 s.

Controlled solvent annealing of the mixture layer is executed in an upright column. Three solvents bromobenzene (BB), 1,2-dichlorobenzene (ODCB), and 2-chlorophenol (CP) were used in this work. In this process, solvent is added to the bottom of 100 cm long vertical column and allowed to equilibrate for 6 hours, forming a linear vapor pressure gradient along the length of the column. In this column, the solvent vapor pressure is zero at the top of the column and the vapor pressure of the solvent at the solvent surface. The amount of solvent vapor that the PCPDTBT/PCBM samples are exposed to is then controlled by the amount of time that the sample is in the column as well as the height at which it resides. The samples in this study are all left at a height that is 90% down the column for 4 hours.

Small-Angle Neutron Scattering: The small angle neutron scattering experiments (SANS) experiments were completed on the General Purpose SANS instrument at the High Flux Isotope Reactor at Oak Ridge National Laboratory and on the NG3 30m SANS instrument at the National Center for Neutron Research at the National Institute for Standards and Technology. The raw data were corrected for scattering from the empty cell, detector dark current, and detector sensitivity. The corrected data were then normalized to an absolute scale using a Porasil-A standard. A stack of 12 or more spin-coated layers was used for each SANS experiment. The scattering length density of PCPDTBT and PCBM are 1.1×10^{-6} Å^{-2} and 4.4×10^{-6} Å^{-2}, respectively.[38,39]

UV-Vis spectroscopy (UV-Vis) spectra were recorded with a Thermo Scientific Evolution 600 UV-Vis spectrophotometer. The solubility of PCBM and PCPDTBT in different solvents was also determined by UV-Vis. The Beer-Lambert law describes the linear relationship between the optical density and solution concentration: $D = c \cdot \varepsilon \cdot L$, where D is the measured optical density, c is the concentration of solution, ε is the extinction coefficient, and L is the path-length, which is 1 mm in this work. The optical densities at 600 nm of PCBM solutions in different solvents of known concentration are measured and plotted as a function of PCBM concentration, and fit to a line. To obtain the PCBM solubility limit, a saturated solution is filtered and serially diluted (30×). The

dilution is necessary because the saturated solution is too dark for transmission of the UV. The optical density of this diluted solution is then recorded, from which the PCBM concentration is determined based on the previously determined extinction coefficient and Beer's law. Finally, the PCBM solubility limit is obtained by multiplying this concentration by 30. The solubility of PCPDTBT is determined by a similar procedure.

Photovoltaic Device Fabrication and Characterization: Indium tin oxide (ITO) glass substrates were first washed with detergent and then cleaned in an ultrasonic bath using DI water, acetone and isopropyl alcohol (IPA). The cleaned substrates were subsequently treated with UV Ozone for 20 minutes. Filtered PEDOT:PSS (Baytron P 4083) was then spin cast on the UV-treated ITO glass at 4000 rpm for 40 s. After baking the PEDOT:PSS films in air at 140 °C for 20 min, the active layer was spin cast at the same condition as above. Solvent annealing of the active layers were carried out at the same conditions as described above. Finally, to create the OPV device, 40 nm of Ca and 60 nm of Al were thermally deposited on the film through a shadow mask. Current-voltage (*I*–*V*) characterization of the polymer photovoltaic cells was conducted using a Thermal Oriel 96000 300-W solar simulator under the illumination of AM1.5G, 100 mW/cm^2. Ten devices were tested for each condition.

Acknowledgements

The authors wish to acknowledge the Sustainable Energy Education Research Center and the Joint Institute for Neutron Sciences at the University of Tennessee, as well as the National Science Foundation (DMR-1005987) for support of this project. MDD also acknowledges the support of the Department of Energy, Office of Basic Energy Sciences, Division of Materials Sciences and Engineering. The support of the Scientific User Facilities Division, Office of Basic Energy Sciences, US Department of Energy, who sponsors the Oak Ridge National Laboratory High Flux Isotope Reactor is gratefully acknowledged. This work also utilized facilities supported in part by the National Science Foundation under Agreement No. DMR-0944772. We acknowledge the support of the National Institute of Standards and Technology, US Department of Commerce, in providing the neutron research facilities used in this work.

Received: February 17, 2014
Revised: March 20, 2014
Published online: May 26, 2014

[1] G. Yu, J. Gao, J. C. Hummelen, F. Wudl, A. J. Heeger, *Science* **1995**, *270*, 1789.
[2] J. Peet, J. Y. Kim, N. E. Coates, W. L. Ma, D. Moses, A. J. Heeger, G. C. Bazan, *Nat. Mater.* **2007**, *6*, 497.
[3] G. Li, V. Shrotriya, Y. Yao, J. S. Huang, Y. Yang, *J. Mater. Chem.* **2007**, *17*, 3126.
[4] G. Li, V. Shrotriya, J. S. Huang, Y. Yao, T. Moriarty, K. Emery, Y. Yang, *Nat. Mater.* **2005**, *4*, 864.
[5] L. M. Chen, Z. R. Hong, G. Li, Y. Yang, *Adv. Mater.* **2009**, *21*, 1434.
[6] S. Günes, H. Neugebauer, N. S. Sariciftci, *Chem. Rev.* **2007**, *107*, 1324.
[7] C. J. Brabec, N. S. Sariciftci, J. C. Hummelen, *Adv. Funct. Mater.* **2001**, *11*, 15.
[8] H. P. Chen, J. H. Chen, W. Yin, X. Yu, M. Shao, K. Xiao, K. L. Hong, D. Pickel, M. Kochemba, S. M. Kilbey, M. D. Dadmun, *J. Mater. Chem. A* **2013**, *1*, 5039.
[9] H. Hoppe, N. S. Sariciftci, *J. Mater. Chem.* **2006**, *16*, 45.
[10] D. Motaung, G. Malgas, C. Arendse, C. Oliphant, D. Knoesen, *J. Mater. Sci.* **2009**, *44*, 3192.
[11] X. N. Yang, J. Loos, S. C. Veenstra, W. J. H. Verhees, M. M. Wienk, J. M. Kroon, M. A. J. Michels, R. A. J. Janssen, *Nano Lett.* **2005**, *5*, 579.
[12] H. J. Kim, H. H. Lee, J. J. Kim, *Macromol. Rapid Commun.* **2009**, *30*, 1269.
[13] Y. Zhao, Z. Y. Xie, Y. Qu, Y. H. Geng, L. X. Wang, *Appl. Phys. Lett.* **2007**, *90*, 043504.
[14] J. Jo, S. I. Na, S. S. Kim, T. W. Lee, Y. Chung, S. Y. Kang, D. Vak, D. Y. Kim, *Adv. Funct. Mater.* **2009**, *19*, 2398.
[15] S. S. Van Bavel, E. Sourty, G. de With, J. Loos, *Nano Lett.* **2009**, *9*, 507.
[16] G. Li, Y. Yao, H. Yang, V. Shrotriya, G. Yang, Y. Yang, *Adv. Funct. Mater.* **2007**, *17*, 1636.
[17] E. Verploegen, C. E. Miller, K. Schmidt, Z. N. Bao, M. F. Toney, *Chem. Mater.* **2012**, *24*, 3923.
[18] Y. Gu, C. Wang, T. P. Russell, *Adv. Energy Mater.* **2012**, *2*, 683.
[19] T. Wang, A. J. Pearson, A. D. F. Dunbar, P. A. Staniec, D. C. Watters, H. Yi, A. J. Ryan, R. A. J. Jones, A. Iraqi, D. G. Lidzey, *Adv. Funct. Mater.* **2012**, *22*, 1399.
[20] Z. M. Beiley, E. T. Hoke, R. Noriega, J. Dacuna, G. F. Burkhard, J. A. Bartelt, A. Salleo, M. F. Toney, M. D. McGehee, *Adv. Energy Mater.* **2011**, *1*, 954.
[21] J. A. Bartelt, Z. M. Beiley, E. T. Hoke, W. R. Mateker, J. D. Douglas, B. A. Collins, J. R. Tumblemston, K. R. Graham, A. Amassian, H. Ade, J. M. J. Frechet, M. F. Toney, M. D. McGehee, *Adv. Energy Mater.* **2013**, *3*, 364.
[22] H. P. Chen, S. Hu, H. D. Zang, B. Hu, M. Dadmun, *Adv. Func. Mater.* **2013**, *23*, 1701.
[23] R. Hegde, N. Henry, B. Whittle, H. Zang, B. Hu, J. Chen, K. Xiao, M. Dadmun, *Solar Energy Mater. Solar Cells* **2012**, *107*, 112.
[24] J. N. Albert, T. D. Bogart, R. L. Lewis, K. L. Beers, M. J. Fasolka, J. B. Hutchison, B. D. Vogt, T. H. Epps, *Nano Lett.* **2011**, *11*, 1351–1357.
[25] K. W. Gotrik, A. F. Hannon, J. G. Son, B. Keller, A. Alexander-Katz, C. A. Ross, *ACS Nano* **2012**, *6*, 8052–8059.
[26] J. N. L. Albert, W. S. Young, R. L. Lewei, T. D. Bogart, J. R. Smith, T. H. Epps, *ACS Nano* **2012**, *6*, 459–466.
[27] K. W. Gotrik, C. A. Ross, *Nano Lett.* **2012**, *13*, 5117–5122.
[28] X. D. Gu, I. Gunkel, A. Hexemer, W. Y. Gu, T. P. Russell, *Adv. Mater.* **2014**, *26*, 273–281.
[29] J. W. Kiel, A. P. R. Eberle, M. E. Mackay, *Phys. Rev. Lett.* **2010**, *105*, 168701.
[30] G. V. Z. Schulz, *Phys. Chem.* **1939**, *B43*, 25.
[31] S. Kline, *J. Appl. Crystallogr.* **2006**, *39*, 895–900.
[32] W. Yin, M. Dadmun, *ACS Nano* **2011**, *5*, 4756–4768.
[33] R. Mehta, M. D. Dadmun, *Macromolecules* **2006**, *39*, 8799.
[34] P. Debye, A. M. Bueche, *J. Appl. Phys.* **1949**, *20*, 518.
[35] J. Peet, N. S. Cho, S. K. Lee, G. C. Bazan, *Macromolecules* **2008**, *41*, 8655.
[36] Y. Yao, J. H. Hou, Z. Xu, G. Li, Y. Yang, *Adv. Funct. Mater.* **2008**, *18*, 1783.
[37] H. Y. Chen, H. Yang, G. Yang, S. Sista, R. Zadoyan, G. Li, Y. Yang, *J. Phys. Chem. C* **2009**, *113*, 7946.
[38] H. P. Chen, R. Hegde, J. Browning, M. D. Dadmun, *Phys. Chem. Chem. Phys.* **2012**, *14*, 5635.
[39] H. P. Chen, J. Peet, S. Hu, J. Azoulay, G. Bazan, M. Dadmun, *Adv. Funct. Mater.* **2014**, *24*, 140.